# COGNITIVE METHOD FOR DETECTING ANOMALOUS CHANGES IN COSMIC RAY FLUX INTENSITY

**© 2025 O. V. Mandrikova*, B. S. Mandrikova****

*Institute of Cosmophysical Research and Radio Wave Propagation, Far Eastern Branch of the Russian Academy of Sciences (IKIR FEB RAS), Paratunka, Kamchatka region, Russia*

**e-mail: oksanam1@mail.ru*

***e-mail: 555bs5@mail.ru*

Received March 10, 2025

Revised April 28, 2025

Accepted May 22, 2025

**Abstract.** A method for detecting anomalous variations in the cosmic ray flux intensity during geomagnetic storms has been developed. The method contains cognitive rules for choosing solutions and is a synthesis of threshold wavelet filtering with elements of statistical decision theory. Numerical implementation of the method allows one to obtain the best solution, in a certain statistical sense, at the rate of data receipt by the processing system. The work used data from ground-based neutron monitors of high-latitude stations (nmdb.eu). Two periods containing extreme geomagnetic storms of levels G5 and G4 and accompanied by two deep Forbush decreases, recorded on May 11, 2024 and January 01, 2025, are considered. The use of the method made it possible to detect anomalous changes in the cosmic ray flux intensity several hours before the onset of Forbush decreases and the registration of geomagnetic storms.

**Keywords:** *data analysis methods, cosmic rays, Forbush effect, space weather, wavelet transform*

**DOI:** 10.31857/S00167940250509e4

## 1. INTRODUCTION

The creation of new and development of existing methods for analyzing geophysical parameters that allow near-real-time assessment of the state of near-Earth space (NEO) are of growing popularity. This is due to the rapid development of technical ground and space infrastructure, the functioning of which significantly depends on space weather factors [Belov et al., 2004; Kuznetsov, 2014; Larionov et al., 2018; Demyanov and Yasiukevich, 2021]. The main space weather factors determining the state of the ICS are solar flares, high-velocity plasma flows from coronal holes, and coronal mass ejections (CMEs) [Kuznetsov, 2014; Abunina et al., 2022]. In ground-based neutron monitors (NM) data reflecting the intensity of the cosmic ray (CR) flux, such events manifest themselves as Forbush decreases (short-term decreases in the recorded intensity of the CR flux) and

GLE events (increases in the NM count rate resulting from an increase in the number of protons in the primary CR flux). Currently, a number of researchers and scientific groups are actively engaged in the development of methods to detect Forbush Declines (FDs) and their precursors [Wawrzynczak and Kopka, 2018; Abunina et al., 2020; Grigoriev et al., 2022; Lagoyda et al., 2024; Mavromichalaki et al., 2024; Nwuzor et al., 2024; Singh and Badruddin, 2024; Savić et al., 2024].

For example, [Mavromichalaki et al., 2024] presented the results of testing the NKUA and NKUA/IZMIRAN systems. The NKUA/IZMIRAN system, based on the station ring method [Abunina et al., 2020], showed satisfactory results for the analyzed events and detected preliminary increases in the CL flux intensity. In [Savić et al., 2024], differential fluence spectra constructed using the Ellison-Ramati model and Band et al. model were obtained to study the relationship between perturbations in the energetic particle flux caused in the ICS by the arrival of high-velocity plasma fluxes from coronal holes, CMEs, and associated FPs. The study [Savić et al., 2024] showed that the correlation between the spectral indices of the solar energetic particle fluence spectra and strong and moderate FPs (data taken from (http://spaceweather.izmiran.ru)) was found to be significant. In [Kolarski et al., 2023] a study of the impact of a solar flare on the ionosphere and primary cosmic rays was carried out. Numerical modeling revealed a significant change in the ionospheric parameters (gradient of the electron concentration profile and effective reflection height) and an increase in the electron concentration by several orders of magnitude [Kolarski et al., 2023]. This study also showed the dependence of the correlation between heliospheric and geomagnetic parameters on the median CL energy.

In [Getmanov et al., 2024a; b], researchers proposed a new method based on the application of neural networks for the task of forecasting geomagnetic storms. The developed method [Getmanov et al., 2024a] confirmed the hypothesis about the dependence between the time series of matrix observations of the muon hodoscope and *Dst-indices*. Researchers [Getmanov et al., 2019] developed an automated method based on digital processing of data from space monitoring measurement systems for the task of early diagnosis of geomagnetic storms. Statistical evaluations confirmed the effectiveness of this method [Getmanov et al., 2019]. In [Monte-Moreno et al., 2022], a nearest neighbor method is used to predict global ionospheric total electron content (TEC) maps. Unlike neural network methods, this approach [Monte-Moreno et al., 2022] does not require a pre-training procedure. However, the method has been tested on a limited test sample and requires further research. In [Tang et al., 2020], the applicability of a traditional mathematical method (ARPSS model) and two deep learning algorithms was investigated to solve the PES prediction problem. The study [Tang et al., 2020] showed that the deep learning algorithm for strong geomagnetic storms achieves the best accuracy, in contrast to the traditional approach. For weak and moderate events, satisfactory results could not be obtained in [Tang et al., 2020].

Wavelet analysis methods are increasingly used to study CL variations. The advantage of the approach based on wavelet analysis is the absence of a training procedure and the possibility of numerical realization of transformation operations. For example, a combined method for detecting hidden anomalies in galactic cosmic ray variations based on combining spectral-singular data decomposition and wavelet analysis is presented in [Borog et al., 2011]. As shown in [Borog et al., 2011], the use of wavelet analysis makes it possible to calculate the energy of short-period variations on the background of large amplitude noise. Scientists [Baral et al., 2022] proposed the application of discrete wavelet transform to study the spectral features of CL flux intensity during periods of Forbush decreases. The study [Baral et al., 2022] confirmed a strong correlation ($\sim 0.9$) between the relative changes in the CL flux intensity count rate and the solar wind speed and *Dst* indices. The results showed that the delay time, as measured by the *Dst-index*, is several hours. These results are consistent with the studies of the authors of this paper and the results of [Badruddin et al., 2017; 2019; Mavromichalaki et al., 2024]. The negative delay of the *Dst-index* provides a basis for constructing techniques for forecasting geomagnetic storms from CL variation data.

This work is a continuation of the studies [Mandrikova et al., 2021; Mandrikova and Mandrikova, 2021; 2024] and is devoted to the creation of automated tools for analyzing geophysical monitoring data and anomaly detection. A wide range of data analysis methods, including recent advances in artificial intelligence, aims to learn and reproduce the characteristic features of the data. The problem of anomaly detection is usually solved by searching for deviations from the constructed characteristic image. This approach avoids the need to build models to describe anomalies, which, in most cases, is an unsolvable task due to the complexity of the processes that determine them, the variety of forms of anomalies and the insufficiency of the required a priori data. The heuristic basis of this approach does not provide the possibility of obtaining the best solution. Moreover, given the presence of natural disturbances (including correlated), the obtained heuristic solution may turn out to be false and provide the basis for incorrect theoretical judgments. In this paper, in continuation of the theory [Mandrikova et al., 2021; Mandrikova and Mandrikova, 2021; 2024], a new technique for analyzing natural data and detecting anomalies based on the combination of risk theory and wavelet analysis is constructed. The proposed methodology allows to obtain a near-optimal solution in a certain statistical sense at the rate of data arrival to the processing system. The technique contains a developed cognitive rule for selecting a decision about the state of the data and is a synthesis of threshold wavelet filtering with elements of statistical decision theory. The technique also contains a cognitive rule for selecting the best wavelet basis to minimize the data approximation error. The proposed approach is applicable for limited data sets and does not require training procedure.

In this work, using the constructed methodology, we analyzed data on variations in the intensity of the cosmic ray flux and considered the periods containing extreme geomagnetic storms

(levels G5 and G4) and accompanied by two deep Forbush decreases registered on May 11, 2024 and January 1, 2025. The analysis was performed on the basis of data from ground-based neutron monitors of high-latitude and polar stations (https://www.nmdb.eu/). To assess the state of near-Earth space, data of the interplanetary magnetic field (IMF) and solar wind parameters (https://omniweb.gsfc.nasa.gov/), as well as data of the *Dst-index of* geomagnetic activity (https://wdc.kugi.kyoto-u.ac.jp) were used. The developed technique allowed us to analyze in detail the dynamics of CL variations and to detect anomalous changes several hours before the onset of Forbush decreases and moments of registration of geomagnetic storms. The results of the technique also confirmed the occurrence of the GLE event (GLE74) during the first analyzed geomagnetic storm on May 10, 2024.

## 2. TECHNIQUE FOR ANOMALY DETECTION IN THE DATA

The recorded natural time series is considered as

$$f(t) = A(t) + R(t) + e(t) = \sum_m c_m g_m(t) + R(t,\Theta) + e(t), \quad (1)$$

where anomalous component , $A(t) = \sum_m c_m g_m(t) c_m = \langle f, g_m \rangle$ , $g_m$ are basis functions,$\langle\cdot\rangle$ is the sign of scalar product; regular component ,$R(t) = R(t,\Theta)\Theta$ are model parameters,$t$ is time,$e(t)$ is noise.

According to the research task, the anomalous component$A(t)$ of the model (1) contains useful information and is to be identified. Non-parametric representation of the$A(t)$ component is due to the variety of anomaly shapes, which, in their majority, have non-type distribution. This does not allow, using traditional approaches, to build a parametric model$A(t)$ . The use of machine learning methods, including neural network technologies, also does not guarantee an adequate model, due to the lack of representative statistics. The regular component$R(t)$ of the model (1) is not subject to identification in this paper and is considered as a nuisance (the method of identification$R(t)$ is described in [Mandrikova and Mandrikova, 2024]) :

$$f(t) = A(t) + \big(R(t,\Theta) + e(t)\big) = \sum_m c_m g_m(t) + \varepsilon(t), \quad (2)$$

where $\varepsilon(t) = R(t,\Theta) + e(t)$ is a nuisance.

Thus, in this formulation, the problem of identifying the anomalous component$A(t)$ reduces to the problem of testing the simple hypothesis$\Gamma_0$ (no anomaly in the data, data state$s_0$ ), against the simple alternative$\Gamma_1$ (there is an anomaly in the data, data state$s_1$ ). In algorithmic form: observing $f(t), t \in [l, l+L]$ requires making one of the possible decisions $s_\gamma, \gamma = \overline{0.1}$ that the hypothesis$\Gamma_\gamma$ is true. Accepting the hypothesis$\Gamma_1$ is based on the *likelihood ratio* [Levin, 1989]:

$$\frac{W(A(t)|\Gamma_1)}{W(\varepsilon(t)|\Gamma_0)} \geq T, \quad (3)$$

where $W(A(t)|\Gamma_0)$ and $W(\varepsilon(t)|\Gamma_1)$ are the probability densities of the distributions when the hypotheses$\Gamma_0$ and$\Gamma_1$, are true, respectively, and $T$ is the threshold.

Then, having a time series$f(t)$ in the form (2), where the anomalous component$A(t)$ is represented as its expansion over some basis $B = \{g_m\}_{m\epsilon N}$ ($N$ - natural numbers): $A(t) = \sum_m c_m g_m(t)$, the problem of identifying$A(t)$ , according to statement (3), reduces to applying the threshold function P(·) with threshold :$T$

$$\hat{A}(t) = \sum_{m\epsilon N} \Pi(\langle f, g_m\rangle) g_m(t) = \sum_{m\epsilon N} \Pi(c_m) g_m(t), \quad (4)$$

where P . $(c_m) = \begin{cases} c_m, if|c_m| \geq T \\ 0, if|c_m| < T \end{cases}$

The error of operation (4) obviously depends on the value of the threshold$T$ and the approximating basis$B$ . Having ordered the moduli of the coefficients of $\{|c_m|\}_{m\epsilon\mathbb{N}}$ in the basisB in descending order:

$$|c_{\mathrm{B}}[l]| \geq |c_{\mathrm{B}}[l+1]|,$$

where$c_{\mathrm{B}}[l] = c_{m_l}$ , we obtain that the error of operation (4) with threshold :$T_L|c_{\mathrm{B}}[L+1]| < T_L \leq |c_{\mathrm{B}}[L]|$ is

$$\varepsilon[T_L] = \left\|\hat{A}(t) - f(t)\right\|^2 = \sum_{l=L+1}^{+\infty} |c_{\mathrm{B}}[l]|^2. \quad (5)$$

Considering the two-parameter wavelet basis functions [Chui, 1992; Astafieva, 1996]: $\Psi = \{\Psi_{j,n}\}_{(j,n)\epsilon Z^2}$,$j$ is the scale parameter,$n$ is the time parameter, from relation (4) we obtain an estimate of

$$\hat{A}_\Psi(t) = \sum_j \sum_n \Pi_{T_{j,n}}(c_{j,n}) \Psi_{j,n}(t), \quad c_{j,n} = \langle f, \Psi_{j,n}\rangle \quad (6)$$

Then, according to (5), we have the error in the wavelet basis

$$\varepsilon_\Psi[T_{j,n}] = \left\|\hat{A}_\Psi(t) - f(t)\right\|^2 = \sum_{(j,n)\notin I_\Psi} |c_{j,n}|^2, \quad (7)$$

where $I_\Psi$ is the set of indices of wavelet coefficients having amplitudes $|c_{j,n}| = |\langle f, \Psi_{j,n}\rangle| \geq T_{j,n}$.

In this case, according to the results of [DeVore, 1998], for functions$f(t)$ with bounded variation and having an untyped distribution, the error$\varepsilon_\Psi[T_{j,n}]$ of the estimation of the anomalous component$A(t)$ (see (7)) cannot be reduced by any other approximation computed in the orthonormalized basis. Therefore, as noted in [Malla, 2005], in this sense *wavelets are optimal for approximating functions with limited variation, in the case of untyped distributions*. Moreover, according to the results of [Mandrikova and Mandrikova, 2024; Mandrikova, 2024], using a two-

parameter wavelet basis, we obtain the possibility of adapting the threshold$T_{j,n}$ in terms of both the time variable$n$ , and the scale $j$.

Then, from the representation (6), following the results of [Mandrikova and Mandrikova, 2024], we obtain the *best estimate of the anomalous component* $\hat{A}(t)$

$$\hat{A}(t) = \sum_j \sum_n \Pi_{\sigma_{j,n}}(c_{j,n})\Psi_{j,n}(t), \quad (8)$$

where$\Pi_{\sigma_{j,n}}(c_{j,n}) = \begin{cases} c_{j,n}, if|c_{j,n}| \geq h * \sigma_{j,n} \\ 0, if|c_{j,n}| < h * \sigma_{j,n} \end{cases}$ , threshold ,$T_{j,n} = h * \sigma_{j,n}\sigma_{j,n}^2(t) = E\left\{\left|\langle\varepsilon(t), \Psi_{j,n}(t)\rangle\right|^2\right\}$ is the variance of the disturbance$\varepsilon(t)$ at time$t = n$ on the scale ,$jE$ is the expectation matrix.

As shown in [Mandrikova and Mandrikova, 2024; Mandrikova, 2024], an important advantage of operation (8), in contrast to traditional approaches, is the ability to compensate for correlated natural interference . $\varepsilon$

Further, using Jaffard's theorem [Jaffard, 1991] and assuming that the increasing amplitudes of the coefficients$|c_{j,n}|$ determine the occurrence of an anomalous feature in the time series$f(t)$ in the neighborhood of the point$t = n$ and outside the neighborhood containing anomalous features, the values of $|c_{j,n}|$ on the argument$n$ are close to zero (Jaffard):

$$|c_{j,n}| \leq Qk^{q+0.5} \ (Q = \text{const} > 0, q - Lipschitz\ index) \quad (9)$$

we obtain cognitive *rule 1 (data state decision making)*: the *data contain an anomalous feature in the neighborhood of the point*$t = n$ *on the scale*$j$ *, if*$|c_{j,n}|$ *on the scale*$j$ *does not satisfy condition (9) in the neighborhood of this point, and the lowest risk is estimated (see (5))*:

$$\hat{A}(t) = \sum_j \sum_n \Pi_{T_{\alpha,j,n}}(c_{j,n})\Psi_{j,n}(t), \quad (10)$$

*where*$\Pi_{T_{\alpha,j,n}}(c_{j,n}) = \begin{cases} c_{j,n}, if|c_{j,n}| \geq T_{\alpha,j,n} \\ 0, if|c_{j,n}| < T_{\alpha,j,n} \end{cases}$ *, and the threshold*$T_{\alpha,j,n} = h_\alpha * \hat{\sigma}_{j,n}$ *is estimated in the neighborhood of*$(j, n)$ *using the Neyman-Pearson criterion from the condition*$\int_A W(|c_{j,n}||\Gamma_0)d|c_{j,n}| = \alpha$ *, where*$\alpha -$ *is a genus I error* (the circumflex in$\hat{\sigma}$ is used to denote the estimate of the standard deviation, as opposed to its actual value ).$\sigma$

The risk of the estimate (10) is bounded by the value of [Mandrikova and Mandrikova, 2024]

$$R_\Psi\left(\hat{A}(t), A(t)\right) = \sum_{j,n} min\left(|\langle A, \Psi_{j,n}\rangle|^2, \left(\sigma_{j,n}^\Psi\right)^2\right) \leq \sum_{j,n}\left(\sigma_{j,n}^\Psi\right)^2. \quad (11)$$

From relation (11) and according to cognitive rule 1, we obtain *cognitive rule 2* (*selection of the best wavelet basis): using the dictionary of bases* $\Omega = \bigcup_{\lambda \epsilon \Lambda} \mathcal{B}_\lambda$ *, for the input data set* $f(t_n)$ *, we estimate the risk* $R_\Psi\left(\hat{A}(t), A(t)\right)$ *and determine the wavelet basis* $\Psi_{best}$ *, minimizing the risk.*

$$R_{\Psi_{best}}\left(\hat{A}(t), A(t)\right) = \min_{\Psi \in \Omega} R_\Psi\left(\hat{A}(t), A(t)\right) = \min_{\Psi \in \Omega} \sum_{j,n} \left(\sigma_{j,n}^{\Psi}\right)^2.$$

Thus we obtain the following *algorithm for detecting anomalies* in the data:

**Step 1.** Using the set of wavelet bases $D = \bigcup_{\lambda \epsilon \Lambda} \mathcal{B}_\lambda$ , we perform a discrete wavelet transform on the data $f(t)$ :

$$f(t) = \sum_{k=0}^{K} \sum_{n=1}^{N} \langle f(t), \Psi_{k,n}^{\lambda}(t) \rangle \Psi_{k,n}^{\lambda}(t),$$

where $K-$ is the largest analyzed scale, $N$ is the length of the time series.

**Step 2.** Based on *cognitive rule 1,* for each scale $k = \overline{1, K}$ , we obtain an estimate $\hat{A}(t)_{k,\Psi^\lambda}$ :

$$\hat{A}(t)_{k,\Psi^\lambda} = \sum_{n=1}^{N} \Pi_{T_{\alpha,k,n}}\left(\langle f, \Psi_{k,n}^{\lambda} \rangle\right) \Psi_{k,n}^{\lambda}(t),$$

where $\Pi_{T_{\alpha,k,n}}\left(\langle f, \Psi_{k,n}^{\lambda} \rangle\right) = \begin{cases} \langle f, \Psi_{k,n}^{\lambda} \rangle, \text{если} \left|\langle f, \Psi_{k,n}^{\lambda} \rangle\right| \geq T_{\alpha,k,n} \\ 0, \text{если} \left|\langle f, \Psi_{k,n}^{\lambda} \rangle\right| < T_{\alpha,k,n} \end{cases}$ , $T_{\alpha,k,n} = t_{\frac{1-\alpha}{2}} \hat{\sigma}_{k,n}$,

$\hat{\sigma}_{k,n}^{\Psi^\lambda} = \sqrt{\frac{1}{M} \sum_{n=1}^{M} \left(\langle f, \Psi_{k,n}^{\lambda} \rangle - \overline{\langle f, \Psi_{k,n}^{\lambda} \rangle}\right)^2}$ , $\overline{\langle f, \Psi_{k,n}^{\lambda} \rangle}$ is the mean value.

**Step 3.** We perform wavelet restoration of the data to the original resolution:

$$\tilde{f}_{\Psi^\lambda}(t) = \sum_{k=1}^{K} \sum_{n=1}^{N} \Pi_{T_{\alpha,k,n}}\left(\langle f, \Psi_{k,n}^{\lambda} \rangle\right) \Psi_{k,n}^{\lambda}(t).$$

**Step 4.** By *cognitive rule 2,* we select the *best* wavelet basis:

$$\Psi^{best} = argmin_{\Psi^\lambda} \sum_{k,n} \left(\hat{\sigma}_{k,n}^{\Psi^\lambda}\right)^2.$$

**Step 5.** In the best basis $\Psi^{best}$ , for each time instant $t = n$ , we calculate the anomaly intensity:

$$E_n = \sum_{k=1}^{K} \Pi_{T_{\alpha,k,n}}\left(\langle \tilde{f}_{\Psi^{best}}, \Psi_{k,n}^{best} \rangle\right).$$

To evaluate the effectiveness of the proposed methodology, statistical modeling was carried out in this work. Model data were formed similar to neutron monitor data. 1500 model signals were generated, the structure of which corresponded to the NM data (using wavelet decompositions, the trend was extracted) with added anomalies and correlated (pink) or white noise. Noise was added

additively to the model data, and the anomalies had different shape, amplitude, and duration. Figure 1 shows examples of constructed model data with different types of anomalies.

Fig. 1.

Fig. 2.

Fig. 2 shows plots of anomaly detection probabilities based on the performed statistical modeling, the results are presented as a function of signal-to-noise ratio. The analysis of the results, in particular, shows that the probability of detecting an anomaly with a duration of 20 samples is about 80% at a signal-to-noise ratio of 1.5 (with a false alarm rate of $\alpha$ = 0.01).

## 3. RESULTS OF THE METHOD AND DISCUSSION

The data of high-latitude NM stations, which did not contain outliers characteristic of hardware errors and did not have long outliers (more than 10 samples), were used in this work. If there were small gaps in the data, they were filled with median values. In addition, the representativeness of the data was taken into account when forming the data samples in order to be able to obtain reliable results. Data were selected for those periods when measurements of several NMs (at least three stations) were available. Given these requirements, the set of stations may have some differences from event to event. NM data were taken from the source (https://www.nmdb.eu). In the analysis, solar wind density and velocity (SW) data (https://omniweb.gsfc.nasa.gov/), *Bz* (GSM) data of the interplanetary magnetic field (IMF) component ((https://omniweb.gsfc.nasa.gov/), and *Dst*-index data https://wdc.kugi.kyoto-u.ac.jp/) were used to estimate the state of near-Earth space (NE).

Anomaly detection in the CL variation data was performed according to the *proposed methodology*, and the algorithm described above was applied. At an arbitrary point$t = k$ of the NM data time series, the previous daily time interval was used in the calculations, which for the initial minute data is $M = 1440$ counts (parameter$M$ for the estimation of the standard deviation $\hat{\sigma}_{k,n}^{\Psi^{\lambda}}$ in step 2 of the algorithm). To estimate the intensity of the selected anomalies, following the results of earlier studies by the authors [Mandrikova et al., 2021; Mandrikova and Mandrikova, 2022] and in accordance with step 5 of the described algorithm, the following operation was performed for each $t = t_n$ time instant:

$$E_n = \sum_{k=0}^{K} \Pi_{T_{\alpha,k,n}}\left(\left\langle \tilde{f}_{\Psi^{best}}, \Psi_{k,n}^{best} \right\rangle\right).$$

During the first analyzed period on May 8-15, 2024, a geomagnetic storm of extreme power (G5 level) occurred and a GLE event (GLE74) was registered. To evaluate the state of the GLE, we present the NE velocity (Fig. *3a*) and density data (Fig. *3b*), the *Bz* (GSM) component data of the IMF (Fig. *3c*), and the *Dst-index* data of geomagnetic activity (Fig. 3d). Figure *3d* shows the NM data

of Inuvik, Nain, Oulu and Thule stations. The results of applying the methodology to the NM data are shown in Figures *3e-n*. At the beginning of the period under analysis, the state of ECS was very quiet (http://ipg.geospace.ru): On May 8, the NE velocity did not exceed 490 km/sec, the southern component of the IMF fluctuated from *Bz*= -3 to +6 nT. According to the results of data processing (Fig. *3e-n*), the CL flux intensity was within the background variations. At about 14:00 UT on 9 May, at the background of a slight increase of the CB density (Fig. *3b*), an anomalous increase of the CL flux intensity was observed at all analyzed stations (Fig. *3e-n*); at about 3:00 UT on 10 May, the anomaly significantly exceeded the background level (the value$E_n$ at all stations exceeded$9 \cdot 10^3$ u). At about 14:00 UT on May 10 at Nain and Oulu stations (Fig. *3j*, *h*, *l*, *m*), the anomalous increase of CL flux intensity reached its maximum: at Nain station $E_n = 18 \cdot 10^3$ u.*m*.; at Oulu station $E_n = 9.8 \cdot 10^3$ u.m. At 15:00 UT on May 10, the beginning of geomagnetic storm (G5) was registered (https://omniweb.gsfc.nasa.gov). The variations of the southern component of the IMF at this time have significantly increased and the density and velocity of the NE increased significantly (Fig. *3a*). The CL flux intensity at the initial phase of the storm at all analyzed stations began to sharply decrease and reached its minimum around 22:00 UT on May 10, the deep Forbush decrease was about 4 hours (Fig. *3e-n*). According to the polar NM data (https://www.nmdb.eu), a GLE event (GLE74) was registered at 01:50 UT on May 11 (Fig. *3e-n*). The results of the technique show at this period a sharp recovery of the level of CL variations, at this time the *Dst-index* reached its minimum of -409 nTL.

Fig. 3.

Further, on May 11 at 10:00 UT, an interplanetary CME was registered (CME of May 9), the southern component of the IMF varied about *Bz* = -25 nT, the NE velocity began to increase and reached 1000 km/sec (1:00 UT on May 12). During this period, the CL flux intensity at all analyzed stations began to decrease sharply and reached its minimum around 11:30 UT on May 11 (Fig. *3e-n*). The duration of the arisen Forbush decrease, according to the results of data processing, was about a day. The restoration of the level of CL variations was observed at Nain, Oulu and Thule stations in the first part of the day on May 13, with a delay at some stations by several hours (Fig. *3e-n*). Note that in the first half of the day on May 13, according to data of Nain station (Fig. *3l*), the CL flux intensity slightly exceeded the background level, which, according to the observations [Avakyan et al., 2012; Mandrikova and Mandrikova, 2021], can occur at temperate and high latitudes during the period of the restoring phase of the geomagnetic storm. During these hours, we also observe a slight increase in the CB density (Fig. *3b*) and a southward rotation of the *Bz* component of the IMF (Fig. *3c*). Further, the CL flux intensity varied within the background values (Fig. *3e-n*).

Fig. 4.

Fig.4, for the analysis of the results of the methodology during the periods of geomagnetic storms of different strength and nature, shows the processing of data of the neutron monitor of Nain

station for the period April 30 - May 15, 2024. The results are obtained at the rate of data arrival to the processing system. The moments of the onset of geomagnetic storms (according to the *Dst-index* data) are marked in Fig. 4 by vertical dashed lines. The results of the technique, according to the data of the analyzed Nain station, show the beginning of the anomalous decrease of the CL flux intensity in the second half of the day on May 1. Further, around 10:00 UT on 2 May, the CL flux intensity increased anomalously and at the time of registration of the first analyzed event (at 15:00 UT on 2 May) reached the maximum ($E_n \approx 3 \cdot 10^3$ y. e. ). The beginning of the next weak geomagnetic storm was registered at 20:00 UT on May 5. According to the results of processing, the anomalous decrease of the CL flux intensity occurred during the period of the arrival of the accelerated flux, approximately 5-6 h before the moment of registration of this geomagnetic storm. There was a Forbush decrease with a gradual onset, which reached its maximum around 6:00 UT on May 6.

Note that the dynamics of CL variations on the eve and during the periods of geomagnetic storms can differ. On the eve and at the moments of registration of the analyzed events on May 2 and May 10, 2024, the CL flux intensity was anomalously increased. The weak magnetic storm that occurred on May 5, 2024 was preceded by the anomalous decrease of the CL flux intensity.

Fig. 5.

In the next analyzed period (Fig. 5), a strong geomagnetic storm (G4) occurred on January 1, 2025 as a result of the impact of several CMEs. To evaluate the condition of the CME, Figure 5 shows the velocity (Fig. *5a*) and NE density data (Fig. *5b*), the *Bz-component* data of the MMP (Fig. 5c), and the *Dst-index* data (Fig. *5d*). Figure *5d* shows the NM data of Apatity, Oulu and South Pole stations. At the beginning of the analyzed period on December 29-30, 2024, the state of ECS was very quiet. According to the results of the methodology (Fig. *5e-l*), the CL flux intensity on December 29 was within the background values. In the middle of the day on December 30, during the period 11:00-12:00 UT, the *Bz* component of the IMF turned southward (Fig. *5c*), the *Dst-index* values decreased to -12 nT (https://wdc.kugi.kyoto-u.ac.jp) and according to the results of data processing (Fig. *5e*, *g*, *i*, *k*), the variations of CL flux intensity at Oulu and Apatity stations slightly exceeded the background level - one can observe a positive anomaly of small intensity ($E_n \approx 0.45 \cdot 10^3$ y. e. ), lasting about 5 hours.

On the eve of the geomagnetic storm, in the first part of the day on December 31, the *Bz* component of the IMF turned to the south (Fig. *5c)*, at about 12:00 UT at the South Pole and Oulu stations, an anomalous increase of the CL flux intensity was observed (at the South Pole station the value was$E_n \approx 0.95 \cdot 10^3$y. e. ), the duration of the anomaly at the South Pole station was about 6 hours. Further, at 15:00 the interplanetary CME was registered (CME 01:36 UT and 18:12 UT on December 28), the fluctuations of the southern component of the IMF increased to *Bz*= -17 nT, the NE velocity increased to 490 km/s. During this period the variations of CL flux intensity at the South

Pole station exceeded the background level and a positive anomaly appeared (Fig. *5h*, *l*). At the end of the day on December 31, the CL flux intensity began to decrease and around 8:00 UT on January 1, 2025, a Forbush decrease occurred at all analyzed stations, which reached its minimum at 16:30 UT at Apatity and Oulu stations (Fig. *5e*, *g, i*, *k*) and at 21:00 UT at South Pole station (Fig. *5h*, *l*). At 09:00 UT on January 1, 2025, the beginning of a strong geomagnetic storm (G4) was registered. Note that the results of data processing (Fig. *5i-l*) show a strong correlation between the variations of CL flux intensity and Dst-index values during this event.

## 4. CONCLUSIONS

The results of this work have shown the effectiveness of the developed methodology for studying the variations of cosmic rays during solar events and geomagnetic storms. The technique allows us to perform a detailed data analysis and obtain quantitative estimates of the process variability. On the example of the considered events, the possibility of using the technique in operational data analysis and space weather forecasting was also confirmed. In addition, the study showed the need for an integrated approach to solve space weather problems. The complex dynamics of GCR during perturbed periods and the presence of disturbances require the development of methods for data recording, analysis and interpretation, using modern mathematical tools and computational technologies.

On the example of the considered events, we confirmed the possibility of anomalies of different intensity and duration in the CL variations on the eve of Forbush decreases and geomagnetic storms. In spite of the differences in the data of different neutron monitors, the signs of the general dynamics of the process during the analyzed events are highlighted. The detected anomalies in the CL variations correlated with the data on the state of the interplanetary medium and magnetosphere. The formation of anomalies in CL coincided in time with the arrivals of high-speed accelerated flows. The results are consistent with earlier work by the authors [Mandrikova et al., 2021; Mandrikova and Mandrikova, 2021; 2022] and the results of other researchers [Munakata et al., 2000; Dorman et al., 2005; Badruddin et al., 2017; 2019; Abunina et al., 2020; Mavromichalaki et al., 2024]. This indicates the validity of the results and confirms the importance of considering GCR when performing space weather forecasting.

In addition, the study showed some differences in the dynamics of CL variations during geomagnetic storms. It is noted that on the eve and during the onset of the events on May 2 and May 10, 2024, the CL flux intensity was anomalously elevated. A weak magnetic storm on May 5, 2024 was preceded by an anomalous decrease in the CL flux intensity. The possibility of occurrence of both an anomalous increase in the CL flux intensity and its anomalous decrease is also confirmed by the works of other scientists [Badruddin et al., 2019; Belov et al., 2015; Homola et al., 2020].

On the eve of the extreme geomagnetic storm on May 10, 2024, the anomalous increase of the CL flux intensity at all analyzed NM stations significantly exceeded the background level (the value of$E_n$ exceeded$9 \cdot 10^3$ uC). The event on 1 January 2025 (level G4) was preceded by insignificant anomalous changes in the variations of cosmic rays, which exceeded the background level only at the polar station South Pole (the value$E_n \approx 0.95 \cdot 10^3$ u.u.) and at the other analyzed stations were within the background.

A detailed analysis of the event on January 1, 2025 showed a strong correlation between the variations of the CL flux intensity and the *Dst-index* values. This result is similar to the study [Mandrikova et al., 2023] during a strong geomagnetic storm on March 23, 2023 (G3 level). It is also consistent with the work of other researchers [Badruddin et al., 2017; 2019; Mavromichalaki et al., 2024] and supports the theory of [Badruddin et al., 2019] about the possibility of predicting magnetic storms from CL flux data.

ACKNOWLEDGEMENTS

The authors would like to thank the supporting institutes of the neutron monitor stations (https://www.nmdb.eu, http://spaceweather.izmiran.ru) and the Interplanetary Environment (https://omniweb.gsfc.nasa.gov/ow.html) and *Dst-index of* geomagnetic activity (https://wdc.kugi.kyoto-u.ac.jp) data used in this work.

FUNDING

The work was carried out at the expense of the State Assignment of IKIR FEB RAS (reg. No. of the topic 124012300245-2).

REFERENCES

1. *Abunina M.A., Belov A.V., Eroshenko E.A., Abunin A.A., Oleneva V.A., Yanke V.G., Melkumyan A.A.* Station ring method in the study of cosmic ray variations: 1. General description // Geomagnetism and Aeronomy. V. 60. № 1. P. 41-48. 2020. https://doi.org/10.31857/S0016794020010022

2. *Abunina M.A., Belov A.V., Shlyk N.S., Abunin A.A.* Forbush effects created by solar matter ejections with magnetic clouds / Proceedings of the International Baikal Youth Scientific School on Fundamental Physics. Irkutsk: ISPP SB RAS. P. 21-23. 2022.

3. *Avakyan, S.V.; Voronin, N.A.; Dubarenko, K.A.* Influence of the magnetic storms on the accident rate of the electric power engineering, automation and communication systems (in Russian) // Scientific and Technical Bulletins of St. Petersburg State Polytechnic University. № 3-2 (154). P. 253-266. 2012.

4. *Astafieva, N.M.* Wavelet-analysis: basics of the theory and examples of application (in Russian) // Uspekhi physicheskikh nauki. V. 166. № 11. P. 1145-1170. 1996.
5. *Belov A.V., Villoresi D., Dorman L.I., Eroshenko E.A., Levitin A.E., Parisi M., Ptitsyna N.G., Tyasto M.I., Chizhenkov V.A., Yucci N., Jahnke V.G.* Influence of Space Environment on the Operation of Artificial Earth Satellites // Geomagnetism and Aeronomy. V. 44. № 4. P. 502-510. 2004.
6. *Belov A.V., Eroshenko E.A., Gushchina R.T., Dorman L.I., Oleneva V.A., Yanke V.G.* Cosmic ray variations as a tool for studying solar-terrestrial relations / Electromagnetic and Plasma Processes from the Sun's Interior to the Earth's Interior. Jubilee Collection IZMIRAN-75. V. 1. Ed. V.D. Kuznetsov. MOSCOW: IZMIRAN. P. 258-284. 2015.
7. *Borog V.V., Kryanev A.V., Udumyan D.K.* Combined method for detecting hidden anomalies in the variations of galactic cosmic rays // Geomagnetism and Aeronomy. V. 51. № 4. P. 481-484. 2011.
8. *Getmanov V.G., Gvishiani A.D., Peregudov D.V., Yashin I.I., Solovyov A.A., Dobrovolsky M.N., Sidorov R.V.* Early diagnosis of geomagnetic storms based on observations of space monitoring systems // Solar-Terrestrial Physics. V. 5. № 1. P. 59-67. 2019. https://doi.org/10.12737/szf-51201906
9. *Getmanov V.G., Gvishiani A.D., Solovyov A.A., Zaitsev K.S., Dunayev M.E., Ekhlakov E.V.* Method of geomagnetic storm forecasting based on deep learning neural networks using time series of matrix observations of the URAGAN muon hodoscope // Geomagnetism and Aeronomy. V. 64. № 6. P. 822-839. 2024a. https://doi.org/10.31857/S0016794024060104
10. *Getmanov V.G., Gvishiani A.D., Solov'ev A.A., Zaitsev K.S., Dunayev M.E., Ekhlakov E.V.* Recognition of geomagnetic storms on the basis of matrix time series of observations of the URAGAN muon annualscope using deep learning neural networks // Solar-Terrestrial Physics. V. 10. № 1. P. 83-91. 2024б. https://doi.org/10.12737/szf-101202411.
11. *Grigoriev V.G., Gerasimova S.K., Gololobov P.Yu., Starodubtsev S.A., Zverev A.S.* Features of sporadic variations of density and anisotropy of galactic cosmic rays in the 24th solar activity cycle // Solar-Terrestrial Physics. V. 8. № 1. C. 34-38. 2022. https://doi.org/10.12737/szf-81202204
12. *Demyanov V.V., Yasyukevich Yu.V.* Space weather: risk factors for the global navigation satellite systems (in Russian) // Solar-Terrestrial Physics. V. 7. № 2. P. 30-52. 2021. https://doi.org/10.12737/szf-72202104
13. *Kuznetsov V.D.* Space weather and risks of space activity // Kosmicheskiy tekhnika i tekhnologii. № 3(6). P. 3-13. 2014.

14. *Lagoyda I.A., Voronov S.A., Mikhailov, V.V.* Peculiarities of Forbush decreases from the data of satellite and ground-based detectors // Nuclear Physics. V. 87. № 2. P. 86-90. 2024. https://doi.org/10.31857/S0044002724020036
15. *Larionov I.A., Malkin E.I., Marapulets Yu.V., Mishchenko M.A., Solodchuk A.A.* Layout of the automated hardware-software complex for operational monitoring, identification and analysis of geophysical signals // Vestnik KRAUNTS. Physics and Mathematical Sciences. № 4 (24). P. 213-225. 2018. https://doi.org/10.18454/2079-6641-2018-24-4-213-225
16. *Levin B.R.* Theoretical bases of statistical radio engineering. Moscow: Radio and communication, 653 p. 1989.
17. *Malla S.* Wavelets in signal processing. Moscow: Mir, 671 p. 2005.
18. *Mandrikova O.V., Rodomanskaya A.I., Mandrikova B.S.* Application of a new wavelet decomposition technique for the analysis of geomagnetic data and cosmic ray variations // Geomagnetism and Aeronomy. V. 61. № 4. P. 428-444. 2021. https://doi.org/10.31857/S0016794021030111
18. *Mandrikova O.V.* Intelligent methods of natural data analysis: application to space weather // Computer Optics. V. 48. № 1. P. 139-148. 2024. https://doi.org/10.18287/2412-6179-CO-1367
19. *Badruddin B., Basurah H., Derouich M.* Study of the geoeffectiveness of interplanetary magnetic clouds // Planet. Space Sci. V. 139. P. 1–10. 2017. https://doi.org/10.1016/j.pss.2017.03.001
20. *Badruddin B., Aslam O.P.M., Derouich M., Asiri H., Kudela K.* Forbush decreases and geomagnetic storms during a highly disturbed solar and interplanetary period, 4–10 September 2017 // Space Weather. V. 17. N 3. P. 487–496. 2019. https://doi.org/10.1029/2018SW001941
21. *Baral R., Adhikari B., Calabia A., Shah M., Mishra R., Silwal A., Bohara S., Manandhar R., Peral L., Frías M.D.R.* Spectral features of Forbush decreases during geomagnetic storms // J. Atmos. Sol.-Terr. Phy. V. 242. ID 105981. 2022. https://doi.org/10.1016/j.jastp.2022.105981
22. *Dorman L.I.* Space weather and dangerous phenomena on the Earth: principles of great geomagnetic storms forcasting by online cosmic ray data // Ann. Geophys. V. 23. N 9. P. 2997–3002. 2005. https://doi.org/10.5194/angeo-23-2997-2005
23. *Chui C.K.* An Introduction to Wavelets. NY: Academic Press, 264 p. 1992.
24. *DeVore R.A.* Nonlinear approximation // Acta Numer. V. 7. P. 51–150. 1998. https://doi.org/10.1017/S0962492900002816
25. *Jaffard S.* Pointwise smoothness, two-microlocalization and wavelet coefficients // Publ. Mat. V. 35. N 1. P. 155–168. 1991.
26. *Homola P., Beznosko D., Bhatta G. et al.* Cosmic-ray extremely distributed observatory // Symmetry. V. 12. N 11. ID 1835. 2020. https://doi.org/10.3390/sym12111835

27. *Kolarski A., Veselinović N., Srećković V., Mijić Z., Savić M., Dragić A.* Impacts of extreme space weather events on September 6th, 2017 on ionosphere and primary cosmic rays // Remote Sens. V. 15. N 5. ID 1403. 2023. https://doi.org/10.3390/rs15051403
28. *Mandrikova O., Mandrikova B., Rodomanskay A.* Method of constructing a nonlinear approximating scheme of a complex signal: Application pattern recognition // Mathematics. V. 9. N 7. ID 737. 2021. https://doi.org/10.3390/math9070737
29. *Mandrikova O., Mandrikova B.* Method of wavelet-decomposition to research cosmic ray variations: Application in space weather // Symmetry. V. 13. N 12. ID 2313. 2021. https://doi.org/10.3390/sym13122313
30. *Mandrikova O., Mandrikova B.* Hybrid method for detecting anomalies in cosmic ray variations using neural networks autoencoder // Symmetry. V. 14. N 4. ID 744. 2022. https://doi.org/10.3390/sym14040744
31. *Mandrikova O., Mandrikova B., Esikov O.* Detection of anomalies in natural complicated data structures based on a hybrid approach // Mathematics. V. 11. N 11. ID 2464. 2023. https://doi.org/10.3390/math11112464
32. *Mandrikova O., Mandrikova B.* Hybrid model of natural time series with neural network component and adaptive nonlinear scheme: Application for anomaly detection // Mathematics. V. 12. N 7. ID 1079. 2024. https://doi.org/10.3390/math12071079
33. *Mavromichalaki H., Papailiou M.-C., Livada M. et al.* Unusual Forbush decreases and geomagnetic storms on 24 March, 2024 and 11 May, 2024 // Atmosphere. V. 15. N 9. ID 1033. 2024. https://doi.org/10.3390/atmos15091033
34. *Monte-Moreno E., Yang H., Hernández-Pajares M.* Forecast of the global TEC by Nearest Neighbour technique // Remote Sensing. V. 14. N 6. ID 1361. 2022. https://doi.org/10.3390/rs14061361
35. *Munakata K., Bieber J.W., Yasue S.-I., Kato C., Koyama M., Akahane S., Fujimoto K., Fujii Z., Humble J.E., Duldig M.L.* Precursors of geomagnetic storms observed by the muon detector network // J. Geophys. Res. – Space. V. 105. V 12. P. 27457–27468. 2000. https://doi.org/10.1029/2000JA000064
36. *Nwuzor O., Okike O., Okpara P., Chikwendu A., Ekweh A., Akande P.* Investigating the link between space-weather parameters and Forbush decrease // Nigerian Journal of Physics. V. 33. N 3. P. 92–99. 2024. https://doi.org/10.62292/njp.v33i3.2024.294
37. *Savić M., Veselinović N., Maričić D., Šterc F., Banjanac R., Travar M., Dragić A.* Further study of the relationship between transient effects in energetic proton and cosmic ray fluxes induced by coronal mass ejections // Universe. V. 10. N 7. ID 283. 2024. https://doi.org/10.3390/universe10070283

38. *Singh Y., Badruddin B.* Study of short-term periodicities in the occurrence of Forbush decreases: wavelet analysis // Astrophys. Space Sci. V. 369. N 7. ID 66. 2024. https://doi.org/10.1007/s10509-024-04330-6
39. *Tang R., Zeng F., Chen Z., Wang J.-S., Huang C.-M., Wu Z.* The comparison of predicting storm-time ionospheric TEC by three methods: ARIMA, LSTM, and Seq2Seq // Atmosphere. V. 11. N 4. ID 316. 2020. https://doi.org/10.3390/atmos11040316
40. *Wawrzynczak A., Kopka P.* Approximate Bayesian computation for estimating parameters of data-consistent Forbush decrease model // Entropy. V. 20. N 8. ID 622. 2018. https://doi.org/10.3390/e20080622

## FIGURE CAPTIONS

**Fig. 1.** Examples of constructed model data with anomalies.

**Fig. 2.** Results of evaluation of the technique efficiency using model data (anomaly duration is 20 samples).

**Fig. 3.** Results of NM data processing for the period from 08.05.2024 to 16.05.2024: (*a*) solar wind speed (SWS); (*b*) solar wind density (SWD); (*c*) *Bz-component of* the MMP; (*d*) *Dst-index*; (*e*) NM data; (*f*) result of applying step 3 of the algorithm to the data of Inuvik station; (*g*) result of applying step 3 of the algorithm to the data of Nain station; (*h*) result of applying step 3 *of* the algorithm to the data of Oulu station; (*i*) result of applying step 3 *of* the algorithm to the data of Oulu station. Oulu; (*i*) the result of applying step 3 of the algorithm to the data of Thule station; (*j*) the result of applying step 5 of the algorithm to the data of Inuvik station; (*k*) the result of applying step 5 of the algorithm to the data of Inuvik station; (*l*) the result of applying step 5 of the algorithm to the data of Nain station; (*m*) the result of applying step 5 of the algorithm to the data of Oulu station; (*n*) the result of applying step 5 of the algorithm to the data of Thule station.

**Fig. 4.** Results of processing the NM data of Nain station for the period from 30.04.2024 to 16.05.2024.

**Fig. 5.** Results of NM data processing for the period from 29.12.2024 to 03.01.2025: (*a*) solar wind speed (SWS); (*b*) solar wind density (SWD); (*c*) *Bz-component of* the IMF; (*d*) *Dst-index*; (*e*) NM data; (*f*) result of applying step 3 of the algorithm to the data of Apatity station; (*g*) result of applying step 3 of the algorithm to the data of Oulu station; (h) result of applying step 3 of the algorithm to the data of South Pole station; (i) result of applying step 5 of the algorithm to the data of Apatity station; (i) result of applying step 5 of the algorithm to the data of South Pole station. Oulu; (*h*) the result of applying step 3 of the algorithm to the data of South Pole station; (*i*) the result of applying step 5 of the algorithm to the data of Apatity station; (*j*) the result of applying step 5 *of* the algorithm to the data of Oulu station; (*l*) the result of applying step 5 of the algorithm to the data of South Pole station.

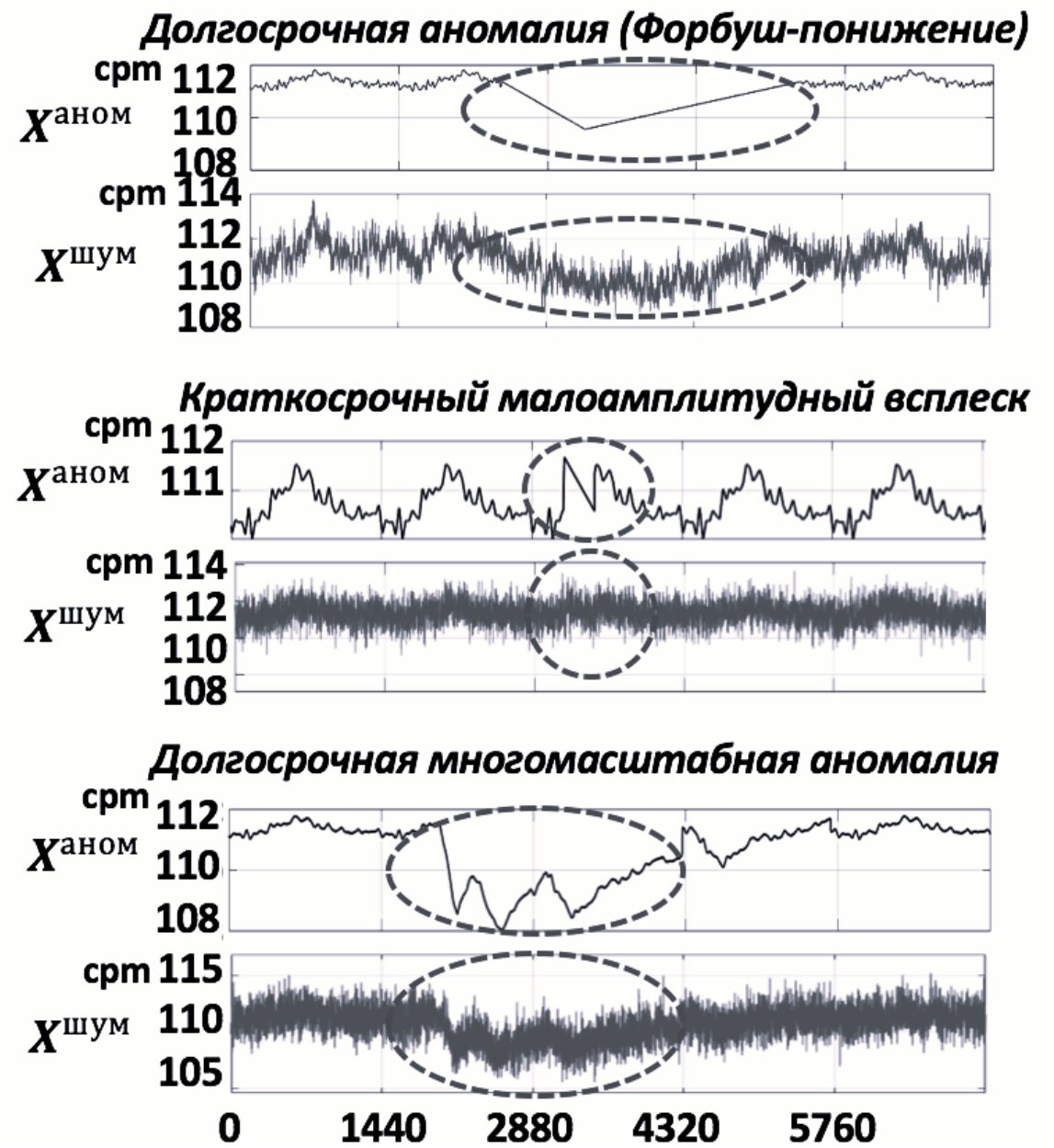
Долгосрочная аномалия (Форбуш-понижение)
cpm
112
110
108
$X^{аном}$
cpm
114
112
110
108
$X^{шум}$
Краткосрочный малоамплитудный всплеск
cpm
112
111
$X^{аном}$
cpm
114
112
110
108
$X^{шум}$
Долгосрочная многомасштабная аномалия
cpm
112
110
108
$X^{аном}$
cpm
115
110
105
$X^{шум}$
0
1440
2880
4320
5760

**Fig. 1.**

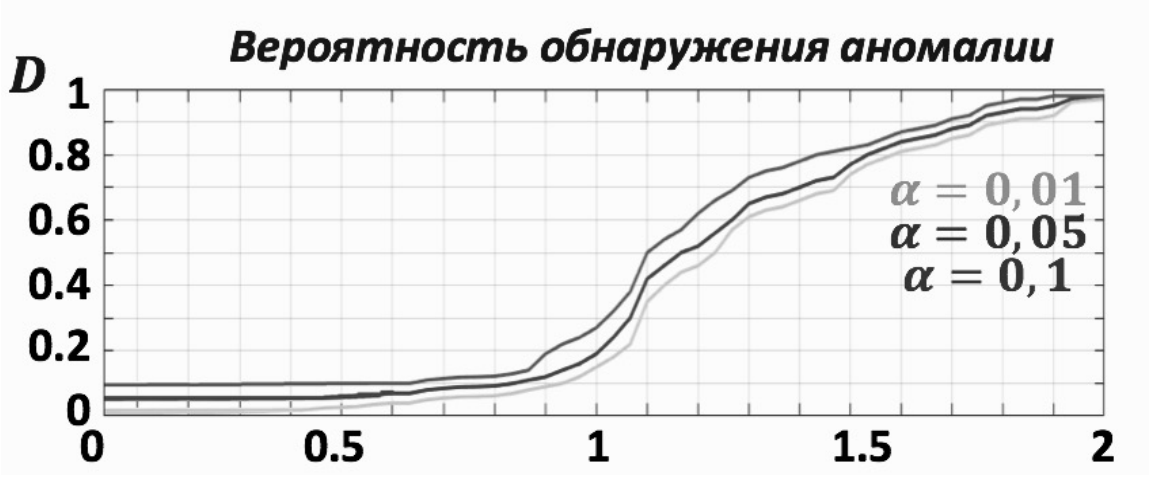
Вероятность обнаружения аномалии
D
1
0.8
0.6
0.4
0.2
0
0
0.5
1
1.5
2
α = 0,01
α = 0,05
α = 0,1

**Fig. 2.**

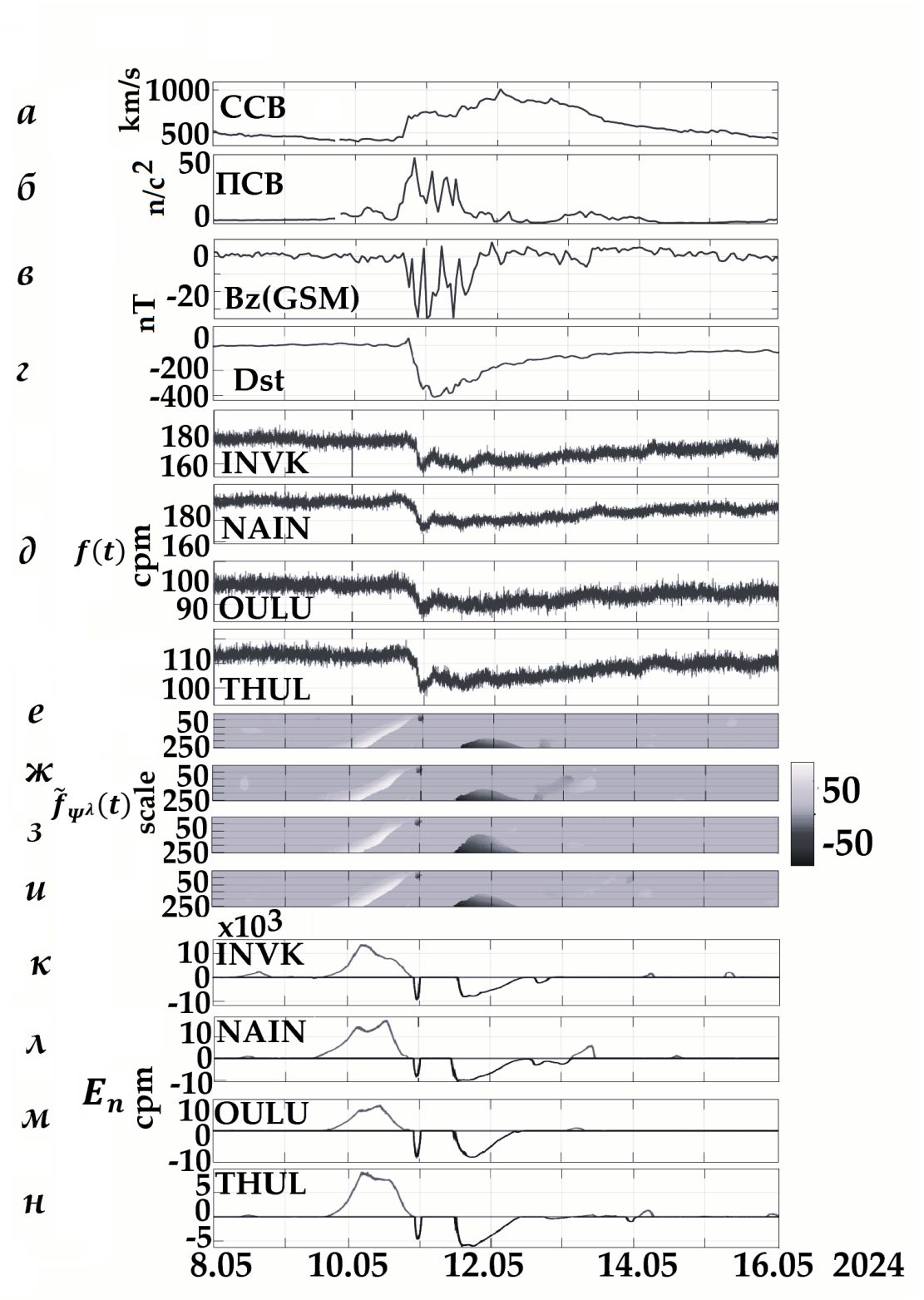
а
km/s
1000
500
ССВ
б
n/c2
50
0
ПСВ
в
0
-20
Bz(GSM)
г
nT
0
-200
-400
Dst
180
160
INVK
180
160
NAIN
д
f(t)
cpm
100
90
OULU
110
100
THUL
е
50
250
ж
50
250
з
50
250
и
50
250
scale
50
-50
x10^3
к
10
0
-10
INVK
л
10
0
-10
NAIN
м
10
0
-10
OULU
н
5
0
-5
THUL
8.05
10.05
12.05
14.05
16.05
2024

**Fig. 3.**

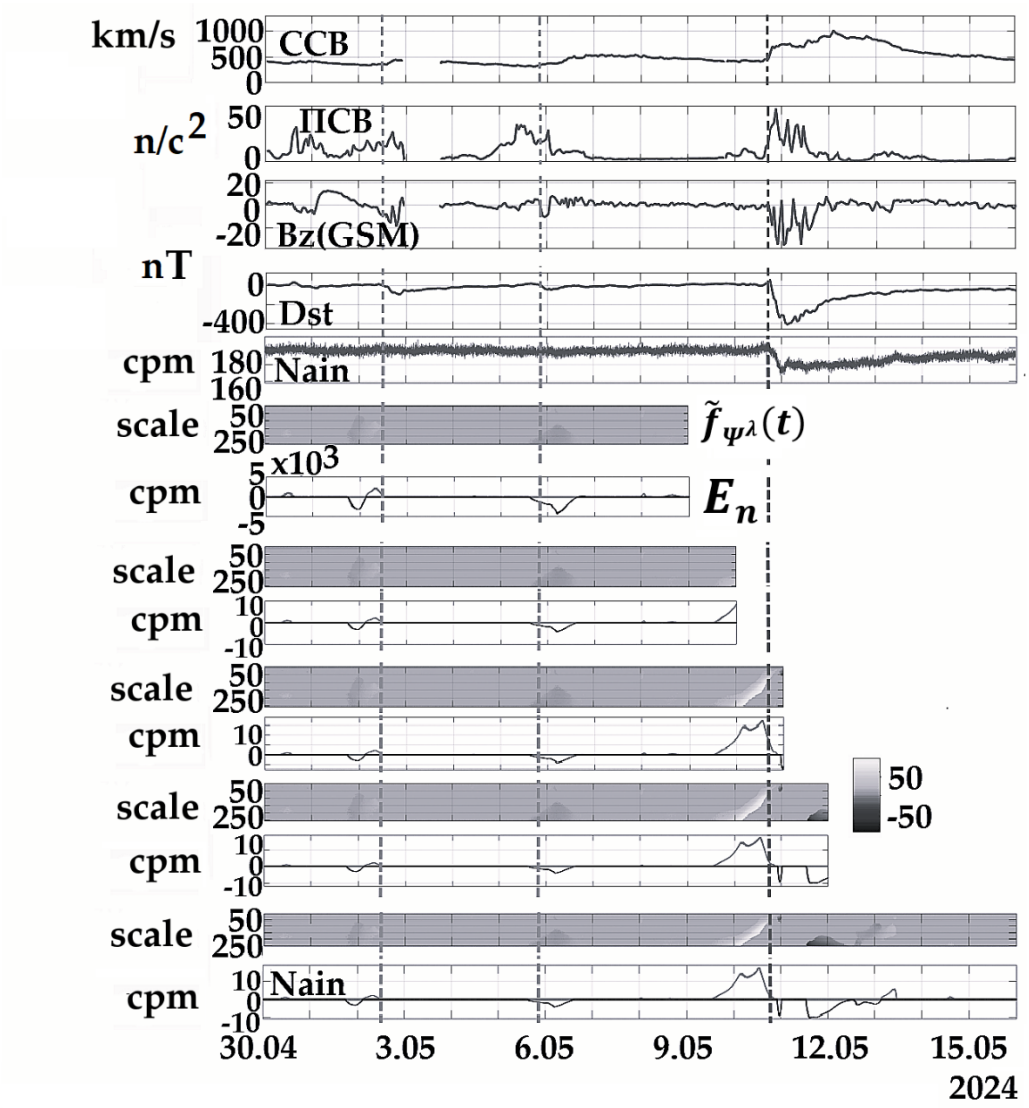
km/s
1000
500
0
CCB
n/c2
50
0
IICB
20
0
-20
Bz(GSM)
nT
0
-400
Dst
cpm
180
160
Nain
scale
50
250
$\tilde{f}_{\psi^\lambda}(t)$
cpm
x10^3
5
0
-5
$E_n$
scale
50
250
cpm
10
0
-10
scale
50
250
cpm
10
0
50
-50
scale
50
250
cpm
10
0
-10
scale
50
250
cpm
10
0
-10
Nain
30.04
3.05
6.05
9.05
12.05
15.05
2024

**Fig. 4.**

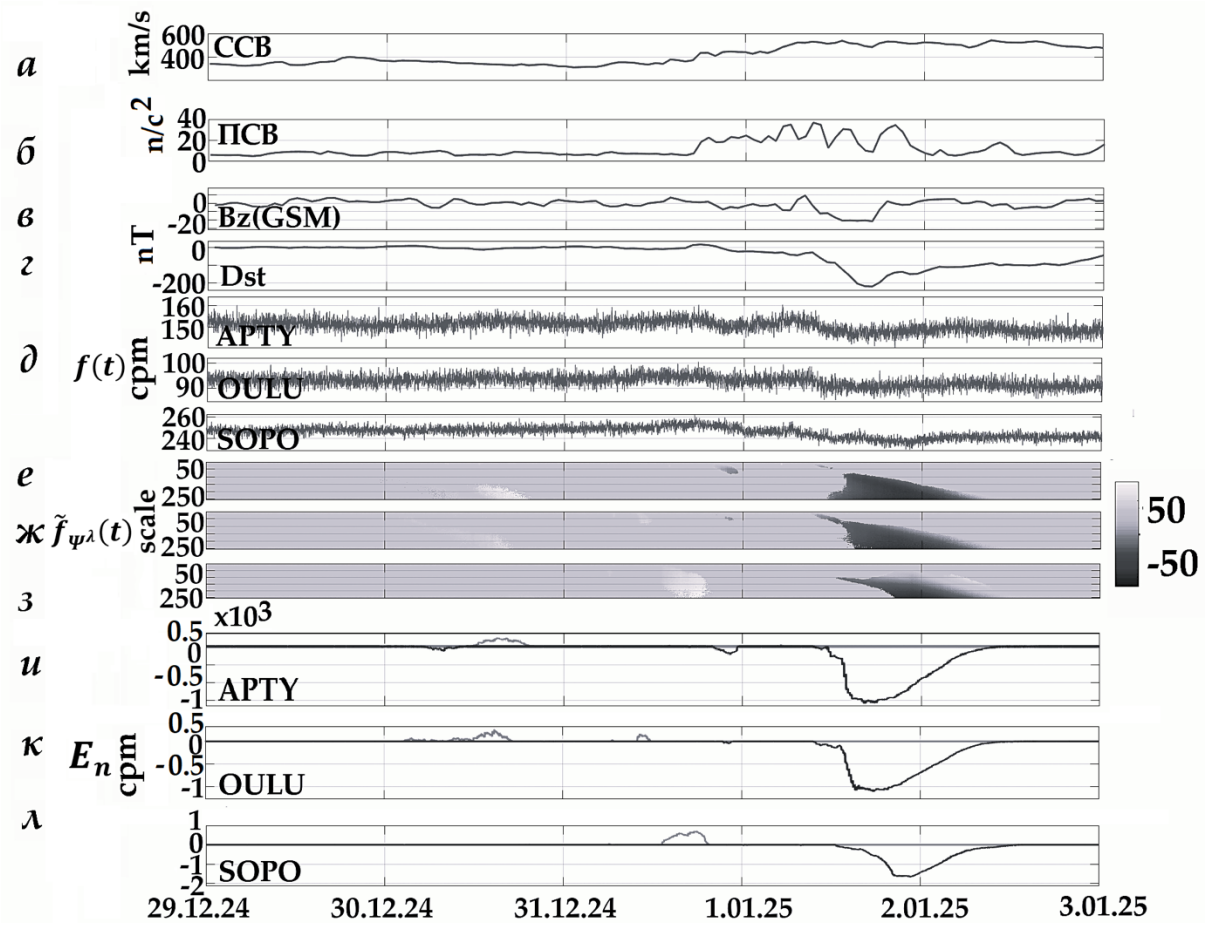
а
km/s
600
400
ССВ
б
n/c2
40
20
0
ПСВ
в
0
-20
Bz(GSM)
г
nT
0
-200
Dst
д
f(t)
cpm
160
150
APTY
100
90
OULU
260
240
SOPO
е
50
250
ж
scale
50
250
50
-50
з
50
250
x10^3
и
0.5
0
-0.5
-1
APTY
к
E_n
cpm
0.5
0
-0.5
-1
OULU
л
1
0
-1
-2
SOPO
29.12.24
30.12.24
31.12.24
1.01.25
2.01.25
3.01.25

**Fig. 5.**